IARJSET ISSN (O) 2393-8021, ISSN (P) 2394-

International Advanced Research Journal in Science, Engineering and Technology

Impact Factor 7.105 ⁜ Vol. 9, Issue 2, February 2022

DOI: 10.17148/IARJSET.2022.9263

Transition Metal Complexes of Ligand containing Aminophenol moiety: Synthesis, Characterization and Antimicrobial Studies of Schiff Base Ligand and its Mixed Ligand Metal Complexes

Sridevi S.P[1], Girija C.R[2], C.D Satish[3], Prashantha Karunakar[4]

[1]Research and Development Centre, Bharatiyar University, Coimbatore, Tamil Nadu – 641046

[2]Dept. of Chemistry, Nrupatunga University/ Govt. Science College, Nrupatunga Road, Bangalore – 560001

[3]Dept. of Science and Humanities, PES University, 100 Feet Ring Road, BSK III Stage, Bangalore – 560085

[4]Department of Biotechnology, PES University, 100 Feet Ring Road, BSK III Stage, Bangalore- 560085

Abstract: A series of metal [Cu(II) and Ni(II) complexes have been prepared with an azo ligand, 2-{E-[4-hydroxyphenyl)imino]methyl}phenol(**SB1**) derived from the Aminophenol nucleus synthesized and along with their complexes were characterized by investigating various spectroscopic and analytical techniques such as UV-Vis, FTIR, ^{1}H NMR, powder- XRD and TGA. The azomethine ligand and its mixed ligand complexes have been investigated for their antimicrobial, anticancer, and DNA binding studies. These tested compounds showed moderate to good antimicrobial activity compared with the standards. MIC studies have revealed that the SB1 ligand is more effective against pathogens.

In addition, all the prepared compounds exhibited a significant groove-binding property to the CT-DNA.

Article info

Keywords: Aminophenol, acetaminophen, Antimicrobial, Molecular docking

I. INTRODUCTION

Aminophenol is considered the intriguing member of the category of substituted anilines [1]. p-Aminophenol derivative (acetaminophen) with analgesic and antipyretic properties similar to those of aspirin [2]. Recently, it has been hypothesized that acetaminophen may be acting via the serotonergic pathways to provide analgesia. Acetaminophen has few side effects in the usual dosage range; no significant GI toxicity or functional changes in platelets occur. It is almost entirely metabolized in the liver and the minor metabolites are responsible for the hepatoxicity seen with overdose [2].

Aminophenol derivatives have attracted much attention from researchers who are working in various fundamental and applied research fields. These molecules have been extensively used in biological domains such as therapeutic agents. The azo compounds of aminophenol are used in analytical chemistry [3].

On the other hand, in general, many metal complexes have been used in the field of pharmaceutical chemistry as potential chemotherapeutic, antimicrobial, neurological, anti-inflammatory, and anticancer agents all over the world [4-6]. The azo ligand containing functional groups such as hydroxyl, amide, etc., has considered the ability to be chelate with many transition metals. Therefore, the chelation of transition metal ions with ligands having hydroxyl functional groups have drawn much more attention in the synthesis of metal complexes for their usage in various fascinating field such as chemical, photochemical, physical, photophysical, and as a catalyst [7-8].

The Istain derivative has six-membered and five-membered heterocyclic ring systems and their chemical structures analogs to the amide moiety present in deoxyribonucleic acid (DNA). Literature reported that aminophenol, isatin, and salicylaldehyde are classes of molecules with less toxicity and hence was used in far more biological applications in the field such as anti-microbial, anti-tumor agents, and anticancerous cells. The derivatives have been used in chelation with various transition metals such as Cu, Ni and used for potential pharmaceutical applications. Further, the synthesized metal complexes containing aminophenol moiety have exhibited potential antimicrobial activity [9-19].

IARJSET ISSN (O) 2393-8021, ISSN (P) 2394-

International Advanced Research Journal in Science, Engineering and Technology

Impact Factor 7.105 ⁜ Vol. 9, Issue 2, February 2022

DOI: 10.17148/IARJSET.2022.9263

In this study, the synthesis of ligand SB1 with aminophenol moiety and its coordination of mixed ligand complexes with metal-acac of Cu (II) and Ni(II) have been reported. The complexes were confirmed by investigating various spectroscopic and analytical techniques like UV-Vis, FTIR, ^{1}H NMR, powder- XRD. The azo ligands and their metal-acac complexes have been tested against biological studies and docking studies.

II. EXPERIMENTAL

2.1 Materials and methods

All the chemicals used in this project were of AR grade were obtained from Sigma-Aldrich private limited, Nice chemicals, and SD-fine chemicals. Melting points were determined using a Gallenkamp melting point apparatus. IR Spectra are recorded using KBr disc on an FTIR Perkin Elmer spectrometer within the range of 4000-400 cm^{-1} and Shimadzu Japan (FTIR, 8400). The solid reflectance spectra of the compounds were recorded in UV-VIS spectrophotometer Perkin Elmer USA-model Lambda 35, ^{1}H NMR with $DMSOd^6$ was recorded on Bruker 400 MHz high-resolution multinuclear FT-NMR. TGA studies using Perkin Elmer USA and Elemental analysis using Variomicro select. XRD data were collected.

2.2 Synthesis of ligand:

2.2.1. Synthesis of 2-{E-[4-hydroxyphenyl)imino]methyl}phenol (SB1)

The azo ligand 2-{E-[4-hydroxyphenyl)imino]methyl}phenol (SB 1) was synthesized according to the following procedure. Salicylaldehyde (1.06 g, 0.01 mol) was taken in 100 mL round bottom flasks, to which 4-aminophenol (1.09g, 0.01 mol) was added with ethanol as a medium. The above mixture was placed for reflux for 2 hr. The resulting Schiff base was separated as light orange crystals. The product obtained was filtered, washed, and recrystallized using ethanol. 70% yield was obtained with melting point 142^0 C. Elemental analysis (CHN) showed % of elements closer value to theoretical value. %C 73.11 (70.24), %H 5.17(5.32), %O 15.02(15.5) and %N 6.6(6.45).

2.2.2: Preparation of Metal $(acac)_2$: Metal acetylacetonate was prepared by a known method.

$Cu(acac)_2$: Copper sulphate (1.2g, 0.02 mol) was dissolved in 50 mL distilled water. A solution of sodium acetylacetonate was prepared by adding dropwise sodium hydroxide (1N) solution of acetylacetone (10 mL, 10 g, 0.10 mol) until the oily emulsion formed dissolves. The copper salt solutions were added to this solution with stirring when light blue coloured crystals of copper acetylacetonate were separated, which was suction filtered and dried (M.P. 210^0 C yield 80%).

$Ni(acac)_2$: Nickel chloride (1.2g, 0.02 mol) was dissolved in 50 mL distilled water. A solution of sodium acetylacetonate was prepared by adding dropwise sodium hydroxide (1N) solution of acetylacetone (10 mL, 10 g, 0.10 mol) until the oily emulsion formed dissolves. The nickel salt solutions were added to this solution with stirring when light green coloured crystals of nickel acetylacetonate were separated, which was suction filtered and dried (M.P. 229^0 C yield 80%)

2.2.3: Preparation of Copper(II) and Nickel II) SB1 mixed ligand acac complex:

Copper(II) –SB1 mixed ligand complex synthesis:

To an ethanolic solution (3.17 g, 0.01 mol) of 2-{E-[4-hydroxyphenyl)imino]methyl}phenol (SB1) was added (2.64 g, 0.01 mol) of copper acetylacetonate dissolved in 20 mL of ethanol, drop-wise, with constant stirring and continue for 20 minutes and the resulting mixture was refluxed for 2 hr. The obtained copper metal complexes (dark orange crystals) were filtered, washed with a small amount of ethanol, and dried over calcium chloride (M.P. 224^0 C, yield 75%). These complexes had a non-ionic character according to the molar conductivity measurements.

Nickel(II) –SB1 mixed ligand complex synthesis:

To an ethanolic solution (3.17 g, 0.01 mol) of 2-{E-[4-hydroxyphenyl)imino]methyl}phenol (SB1) was added (2.56 g, 0.01 mol) of nickel acetylacetonate dissolved in 20 mL of ethanol, drop-wise, with constant stirring and continue for 20 minutes and the resulting mixture was refluxed for 2 hr. The obtained nickel-metal complexes (orange crystals) were filtered, washed with a small amount of ethanol, and dried over calcium chloride (M.P. 210^0 C, yield 80%).

2.3: Molecular docking and dynamics

The selected protein-ligand complex was subjected to molecular dynamics simulation in Gromacs-2019.4. The selected ligands topology was downloaded from the Prodrug server to get the force field coordinates. The system was prepared with vacuum minimized for 1500 steps using the steepest descent algorithm. Then the complex structures were solvated in a cubic periodic box of 0.5 nm with a simple point charge (SPCE) water model. The complex systems were subsequently maintained with an appropriate salt concentration of 0.15 M by adding suitable numbers of Na^+ and Cl^-

IARJSET ISSN (O) 2393-8021, ISSN (P) 2394-

International Advanced Research Journal in Science, Engineering and Technology

Impact Factor 7.105 ⁜ Vol. 9, Issue 2, February 2022

DOI: 10.17148/IARJSET.2022.9263

counter ions. The system preparation was referred to based on a previously published paper. Each resultant structure from the NPT equilibration phase was subjected to a final production run in an NPT ensemble for 100 ns simulation time. Trajectory analysis was performed by using the Gromacs simulation package of Protein RMSD, Ligand RMSD, RMSF, RG, and H-Bond.

2.4: Biological activities:

The pharmacological activity of all the isolated Schiff base ligand and mixed ligand acac compounds were studied by screening done in vitro cup diffusion methods [20]. The pharmacological activity, of the isolated ligand and their metal complexes moulds, were grown on sabouraud dextrose agar (SDA) at 25^0 C for 48 hr and determined by using the agar well diffusion method, and fungal growth was subcultured on nutrient broth for their in vitro testing. 15 mL of molten SDA (45^0 C) was added to 100 µL volume of each compound having a concentration of 100 µL/mL in the DMSO and poured into a sterile Petri plate. The solid appeared at the Petri plate which poisoned agar plates were inoculated at the center with bacterial and fungal plugs (8 mm) obtained from activity growing colony and incubated at 25^0C for 48 hr. The diameter of the bacterial and fungal colonies was measured and expressed as the present zone of inhibition [21].

All the isolated ligand and their metal complexes were tested against the microorganisms such as E.coli, S.Aureus for antibacterial and against A.niger and C.albicans for antifungal behaviors. These biological activities of all the compounds were compared with standard (Gentamycin and Nystatin) and control (DMSO). The minimum inhibitory concentration, MIC, the value was defined as the lowest concentration of the chemical agent giving complete inhibition of visible growth.

2.5 Anti-Microbial Activity

Well diffusion method to check the Minimum Inhibition Concentration (MIC)**:**
Nanoparticle samples (SB1) were assessed in duplicates for their MIC property against organisms.

Sample preparation:
10 mg of Nanoparticle (SB1) were dissolved in 1mL of Dimethyl sulfoxide (DMSO). Different aliquots of the sample were prepared by pipetting 10µL (100µg), 20µL (200µg), 30µL (300µg), and 40µL (400µg), and the final volume was made up to 50µL by adding DMSO.

Media preparation for MIC
For fungal plate- Potato Dextrose Agar (PDA: Potato-200g, Dextrose-20g, Agar-20g, Distilled water-1000mL) 500mL of media was prepared by boiling 100g of Potato in 200mL distilled water and filtered. 10g of Dextrose, 10g of Agar was added into the filtrate and the final volume was made up to 500mL with distilled water.

For bacterial plate-Luria Bertani (LB) agar media (Tryptone 10g, Sodium chloride 10g, Yeast extract 6g, Agar 20g, Distilled water 1000mL) 800mL was prepared by adding Tryptone 8g, Sodium chloride 8g, Yeast extract 4.8g, Agar 16g, Distilled water 800mL and autoclaved at 121°C for 15 min.

Platting for MIC against organisms.
Approximately 25ml of the media (PDA and LB agar) was poured into the sterilized Petri plates and allowed them to solidify. 200µL inoculum (Aspergillus niger, Candida albicans, E-coli, Staphylococcus aureus, and Streptococcus mutans) was poured into the respective PDA and LB agar plates and spread thoroughly using a plate spreader. Five wells measuring 0.5cm were made using the borer in respective plates. 50µL of Nanoparticle sample (SB1) 100µg, 200µg, 300µg, and 400µg are loaded into the respective wells and 50µL of DMSO loaded in the center well as control blank. The bacterial plates were incubated at 37°C for 24hr and the Fungal plates were incubated at 25°C for 72hr. Later, the zone of inhibition was recorded in Mm (millimeter) [22, 23].

III. RESULTS AND DISCUSSION

A series of metal complexes were prepared by using one ligand and the structural studies were carried out by investigating various analytical and spectroscopic techniques such as UV-Vis, elemental analysis, IR, ^{1}H NMR, TGA, powder- XRD. The obtained complexes are coloured and have a higher melting point compared to the ligand and they are thermally stable. The ligand SB1 was found to be more effective towards antimicrobial activities and thus extensive biological studies have been conducted to understand the antimicrobial activities of SB1 and docking studies of SB1 performed.

IARJSET ISSN (O) 2393-8021, ISSN (P) 2394-

International Advanced Research Journal in Science, Engineering and Technology

Impact Factor 7.105 ⁜ Vol. 9, Issue 2, February 2022

DOI: 10.17148/IARJSET.2022.9263

3.1 FT-IR spectra of ligands and their complexes:

SB1 and its Ni-complex: The weak broad bands in the region 3400 cm^{-1} due to hydrogen-bonded OH group. This indicates that the phenolic oxygen atoms present in the Schiff bases are coordinated to the metal centers. The –OH band in SB1 changed significantly upon metal complexation, indicating deprotonation and subsequent involvement of the phenoxyl group in metal coordination as observed in Figure 1. The coordination of the phenolic oxygen atom could be supported by the appearance of medium-to-strong bands at a lower frequency region, 500 cm^{-1}, assignable to frequency (M-OC) vibration. The strong m(C=N) bands occurring in the range of 1794 cm^{-1} are shifted slightly toward lower frequency 1725 cm^{-1} compared to the free Schiff bases indicating the coordinated azomethine nitrogen atom to the metal center. The strong band (N-H) occurring in the range of 3780 cm^{-1} are shifted towards lower frequency 3414 cm^{-1} compared to the free Schiff bases indicating the co-ordinated nitrogen to the metal center. The appearance of strong broadband at 3449 cm^{-1} in the Nickel complex strongly supports the presence of coordinated water molecules. The coordination of oxygen atoms could be supported by the appearance of medium-to-strong bands at a lower frequency region, 445 cm^{-1}, assignable to M-OC vibration. **Fig 1 & 2 attached at the end.**

3.2 Electronic studies:

The electronic absorption spectra of metal complexes are recorded in DMSO in the range of 200 – 800 nm. The electronic spectrum of the free Schiff base revealed three bands around 241, 350, and 450 nm characteristic of π-π * and n-π* transitions. In the metal complexes, this band is shifted to a longer wavelength with increasing intensity. This shift may be attributed to the donation of lone pair of electrons of oxygen of Schiff base to metal ion [24]. The copper complex exhibits bands around 255-300 nm, 350- 355 nm, and 477-498 nm. The broad intense and poorly resolved bands around 350-355 nm may be assigned to LMCT or MLCT. The high-intensity band around 250 nm is of ligand cause assignable to n-π* or π-π* transition. The complex exposed shoulder broad bands in the range of 300-325 nm may be assigned to the d–d transition.

3.3: XRD studies: The powder X-ray diffraction study was carried out; the ligand is crystalline. The Miller indices (hkl) along with observed and calculated dangles, 2θ values, and relative intensities. Space group found to be P 21/c.

The average crystalline sizes of the complexes powder-XRD were calculated using Debye Scherrer equation ($D = K\lambda/\beta Cos\theta$), where D=Particle size, K =Dimensionless shape factor, λ=X-ray wavelength (0.15406 Å), βfull width at half maximum of the diffraction peak, θ=Diffraction angle. In the XRD plot, values determined to be 2 θ= 13.63, FWHM = 0.06224, Particle size (D) = 126.74, hkl max observed to be 9, 20, 17 and hkl index values are 1.45, 7.69, 21.46 respectively.

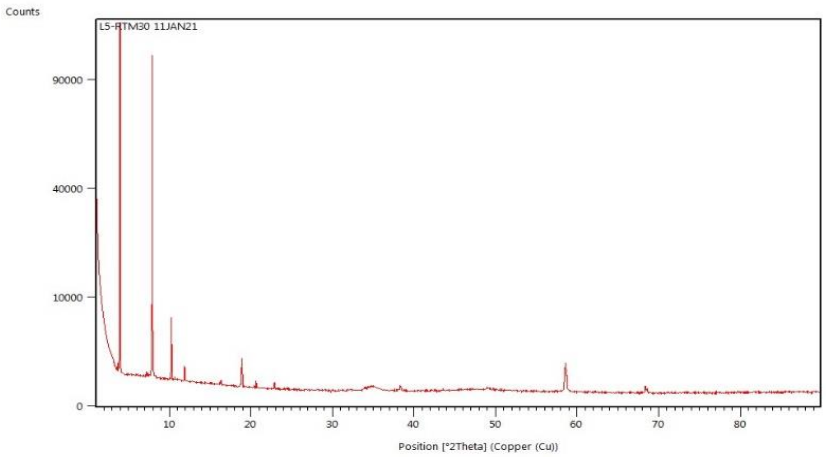

Fig 3(a): XRD plot of SB1 ligand

3.4 ^{1}H NMR spectrum of ligand and its copper complex:

The ^{1}H NMR spectra of representative Schiff base ligands and its mixed ligand acac-complexes. The ligand shows a resonance signal is about 13.5 δ corresponding to the resonance absorption of protons of the -OH group. The observed signals at about 9.0 δ correspond to the azomethine protons of =CH group and signals at 3.8 δ correspond to the hydrogens of the -NH groups of the ligand as observed in Figure 2. The multiplets centers at about 6.9 δ and 7.5 δ are attributed to aromatic protons. In the proton NMR spectra of the metal acac-complex, the azomethine =CH signal is shifted to

IARJSET ISSN (O) 2393-8021, ISSN (P) 2394-

International Advanced Research Journal in Science, Engineering and Technology

Impact Factor 7.105 ⁜ Vol. 9, Issue 2, February 2022

DOI: 10.17148/IARJSET.2022.9263

downfield, as expected, and appears at about 8.6 δ. However, the resonance signals of the protons of the -NH group do not appear, hahaveeen shifted significantly. Whereas, the signals due to the protons of the -OH group of the ligand have diminished in the spectrum of the metal complex indicating the deprotonated form of the ligand and enolization. The observed broad signals of the metal complex indicate the paramagnetic nature of the copper complex.

3.5 Crystal data and structure refinement for SB1.

Identification code	shelf
Empirical formula	$C_{13}H_{11}NO_2$
Formula weight	213.23
Temperature	296(2) K
Wavelength	0.71073 A
Crystal system, space group	Monoclinic, P 21/c
Unit cell dimensions	a = 22.0553(19) A alpha = 90 deg. b = 10.8340(9) A beta = 91.470(2) deg. c = 8.9203(8) A gamma = 90 deg.
Volume	2130.8(3) A^3
Z, Calculated density	8, 1.329 Mg/m^3
Absorption coefficient	0.090 mm^-1
F(000)	896
Crystal size	0.200 x 0.200 x 0.150 mm
Theta range for data collection	3.117 to 24.996 deg.
Limiting indices	-26<=h<=26, -12<=k<=12, -10<=l<=10
Reflections collected / unique	26882 / 3733 [R(int) = 0.0539]
Completeness to theta = 24.996	99.4 %
Absorption correction	Semi-empirical from equivalents
Max.and min. transmission	0.7461 and 0.5915
Refinement method	Full-matrix least-squares on F^2
Data / restraints / parameters	3733 / 0 / 306
Goodness-of-fit on F^2	1.151
Final R indices [I>2sigma (I)]	R1 = 0.0483, wR2 = 0.1122
R indices (all data)	R1 = 0.0571, wR2 = 0.1202
Extinction coefficient	0.063(5)
Largest diff. peak and hole	0.270 and -0.148 e. A^-3

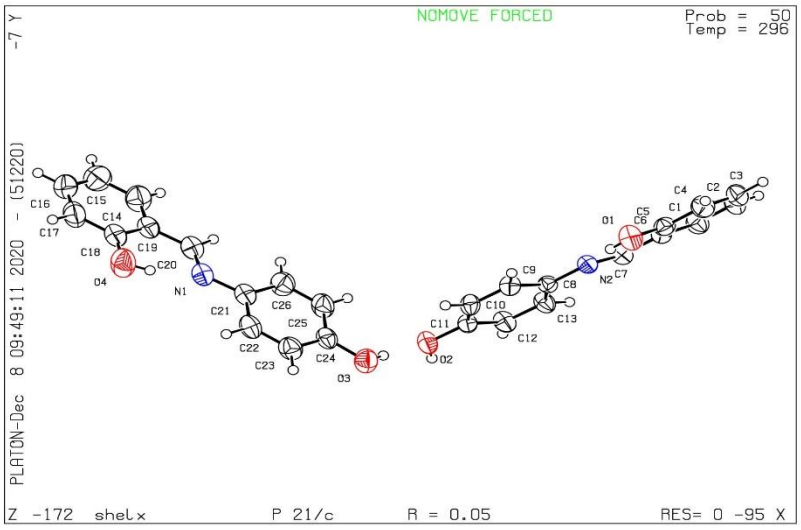

Fig 3(b): ORTEP of SB1

3.6 Hirshfeld surface and 2D fingerprint calculations:

Hirshfeld surfaces are a new graphical approach to visualize intermolecular interactions present in the compounds. The three-dimensional Hirshfeld surfaces are obtained by supplying their crystallographic information files (.cif) into the

IARJSET ISSN (O) 2393-8021, ISSN (P) 2394-

International Advanced Research Journal in Science, Engineering and Technology

Impact Factor 7.105 ⁜ Vol. 9, Issue 2, February 2022

DOI: 10.17148/IARJSET.2022.9263

software Crystal Explorer 3.1[25-27]. The Hirshfeld surfaces were mapped over a norm with the red-white-blue colored scheme, the red and blue colored regions on the d_{norm} surface reveal the atoms with the contact distances are less (−ve d_{norm} value) and more (+ ve d_{norm} value) than the sum of their van der Waals radii, while the white region indicates the contact distance is equal to their van der Waals sum with zero d_{norm}[28]. The appearance of intense bright red coloured circular spots on a d_{norm} surface (Fig.4) highlights the presence of the donor and acceptor elements involved in the hydrogen-bonding interactions.

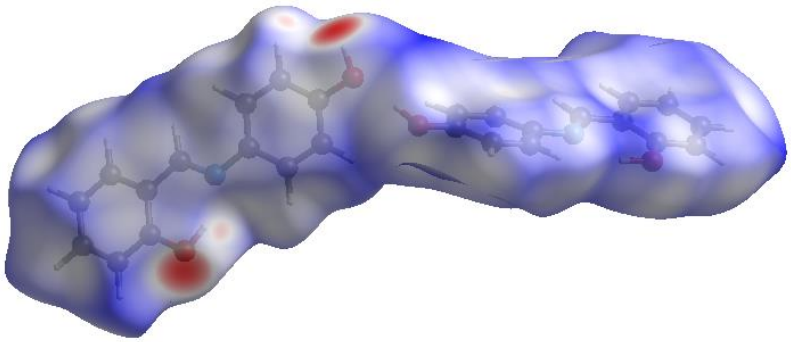

Fig.4. The Hirshfeld surface mapped over d_{norm} in the range -0.6362 to +1.4908 a.u. The circular red spots indicate intermolecular C-H...O interactions.

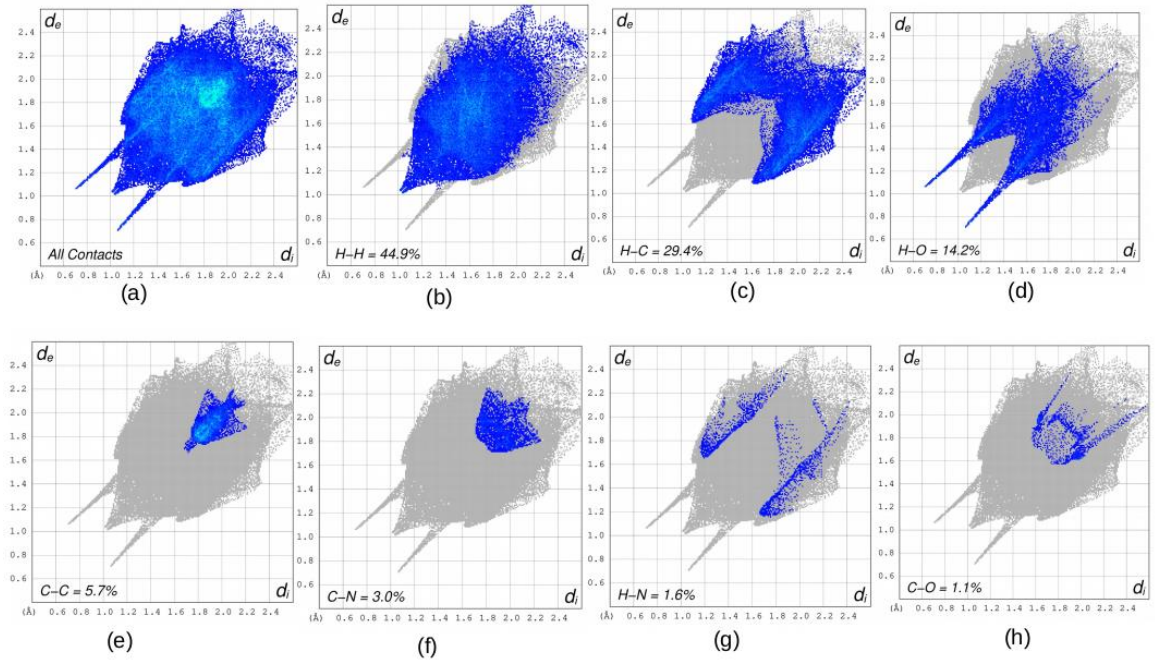

Fig. 5. Two-dimensional fingerprint plots, blue-colored dots indicate the presence of contribution while grey-colored dotted lines show the outline of the fingerprint plots.

The expanded 2D fingerprint plots were displayed in the range of 0.6 – 2.4Å view with the d_e and d_i distance scales displayed on the graph axes as shown in Fig. 5. The d_e and d_i are distances corresponding to the nearest nuclei external and internal to the Hirshfeld surface respectively. The total contribution from all the pairs of contacts was displayed in Fig 5. (a). The results of the 2D fingerprint show that a pair of H...H inter-atomic contacts made the predominant contribution with 44.9% to the three-dimensional Hirshfeld surface. It emerges in the form of blue coloured sharp spoke-like pattern over the region ($d_e+d_i \approx 1.00$Å) delineated in Fig 5. (b). Followed by another major contribution is H...C (Fig. 5c) with 29.4% reflected as a pair of the unique wing-like structures between the region 1.1Å<(d_e+d_i)<1.7Å. A pair of H...O inter-atomic contacts (Fig. 2d) with 14.2% of the contribution, produced a characteristic between the region of 0.7Å<(d_e+d_i)<1.15Å this correlates with the C-H...O intermolecular interaction incurred in the crystal and molecular structure. The C...C inter anointer-atomic spike (Fig. 5e) made 5.7% of contribution which reflected as an arrowhead the

IARJSET ISSN (O) 2393-8021, ISSN (P) 2394-

International Advanced Research Journal in Science, Engineering and Technology

Impact Factor 7.105 ⁜ Vol. 9, Issue 2, February 2022

DOI: 10.17148/IARJSET.2022.9263

region of 1.6Å<(d_e+d_i)<1.7Å. The C...N interactions (Fig. 5f) also were present with the contribution of just 3.0% given out as a convex surface pattern between the region of 1.7Å<(d_e+d_i)<1.82Å. Lastly, H...N, and C...O in inter-atomic contacts are scored with the least contribution of 1.6% and 1.1% as shown in Figures (5g & 5h) respectively. Overall fingerprint calculations reveal that the H...H interactions showed a major role in the formation of a three-dimensional Hirshfeld surface.

3.7 Molecular Dynamics (MD):

In our study, 5IQG protein complex with selected ligands from docking SB1 (PL5) and Gentamicin (GEN) was subjected to molecular dynamics simulation analysis. MD simulation was performed for 100 nanoseconds (ns), to understand the stability of the above ve-mentioned protein-ligand complexes RMSD (Root Mean Square Deviation), RMSF (Root Mean Square Fluctuations), RG (Radius of Gyration), H-Bonds (Hydrogen bonds), and MMPSA calculations were made.

Root mean square deviation

It is an important parameter for the determination of the differences between the two conformations. The higher the RMSD value, the more is the deviation. The RMSD values are calculated against the simulation time scale of 40 to 100ns. The RMSD results for APO and its complex with SB1 and GEN are depicted in figure 6:

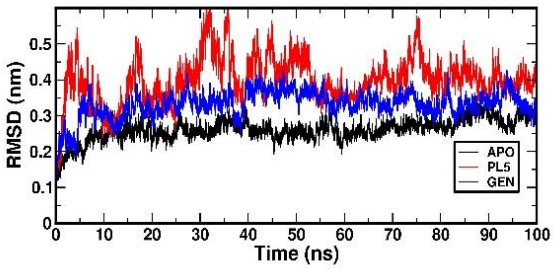

Figure 6: Root means square deviation of backbone atoms of APO and Protein-Ligand complex.

During the 100ns simulation, it was observed that the APO and complexes are equilibrated after 40ns of time. The mean RMSD of the APO and complexes were calculated from 40ns to 100ns. The amino acids involved in bringing the overall structural deviation are explored in the RMSF plots.

Root mean square fluctuation

RMSF analysis determines which amino acids of the protein make more vibrations, resulting in the destabilization of the protein in the presence and absence of the ligands. The RMSF values are calculated against the simulation time scale of 0 to 100ns.

The RMSF results for APO and its complex with PL5 (SB1) and GEN as depicted in figure 6.

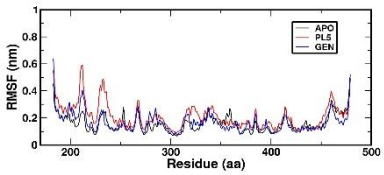

Figure 7: Root means square fluctuation ofc-alpha atoms of APO and its complex with PL5 (SB1) and GEN

The radius of Gyration (RG)

The compactness of the protein can be determined by the radius of gyration. Folding and unfolding of the protein was analyzed by the RG values against the simulation time scale of 0 to 10,000 ps for APO and its complex with PL5 (SB1) and GEN

The RG result of the APO and its complex with PL5 (SB1) and GEN is depicted in Figure 8.

IARJSET ISSN (O) 2393-8021, ISSN (P) 2394-

International Advanced Research Journal in Science, Engineering and Technology

Impact Factor 7.105 ⁜ Vol. 9, Issue 2, February 2022

DOI: 10.17148/IARJSET.2022.9263

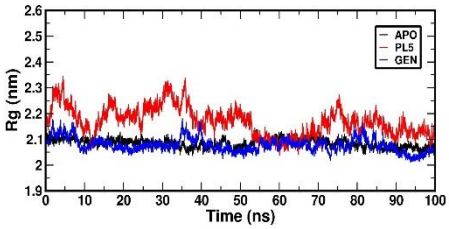

Figure 8: RG of backbone atoms of APO and its complex with PL5 (SB1) and GEN

Hydrogen Bond (H-bond)

Protein-ligand complexes are stabilized by the formation of hydrogen bonds. In our research, the hydrogen bonds formed in the molecular docking analysis are confirmed by the simulation analysis. Here, the total number of hydrogen bonds formed versus the period for APO and its complex with PL5 and GEN are determined.

The H-Bond result of the APO and its complex with PL5 (SB1) and GEN depicted in Figure 9:

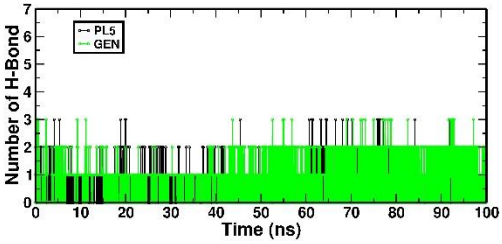

Figure 9: H-bond of APO and its complex with PL5 (SB1) and GEN

MMPBSA

How much energy is required for the ligands to bind to protein is determined by MMPBSA.

Table 1: MMPSA value of 5IQG complex with PL5 (SB1) and GEN of 100ns simulation

Target	Ligand code	Binding energy
5IQG	PL5 (SB1)	-176.249 +/- 16.996 kJ/mol
5IQG	GEN	-124.363 +/- 23.363 kJ/mol

MIC of Sample SB1 against pathogens

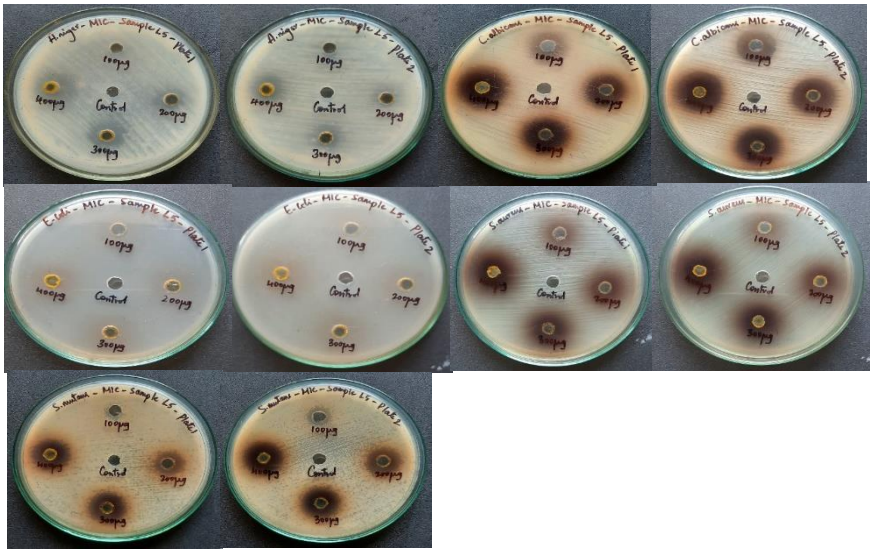

IARJSET ISSN (O) 2393-8021, ISSN (P) 2394-

International Advanced Research Journal in Science, Engineering and Technology

Impact Factor 7.105 ⁜ Vol. 9, Issue 2, February 2022

DOI: 10.17148/IARJSET.2022.9263

Table 2: MIC of Nanoparticle SB 1 against Pathogens

SB 1 in µg/ µL	Zone of inhibition of Pathogens in mm									
	A.niger		C.albicans		E.Coli		S.aureus		S.mutans	
Plates	**1**	**2**	**1**	**2**	**1**	**2**	**1**	**2**	**1**	**2**
100	8	8	16	19	8	8	8	10	10	12
200	13	11	18	20	10	10	10	10	15	16
300	15	13	19	20	12	12	10	10	17	19
400	17	14	20	21	14	14	15	15	18	20
Control				08 mm						
Standard				20 mm						

3.8 Antimicrobial activity:

The results concerning the in vitro antimicrobial activity of the ligand and copper complex, together with the inhibition zone (mm) were discussed.

Table 3: Biological Activity of the Ligand and copper complex:

S.No.	Name	Antibacterial		Antifungal	
		E.Coli	S.Aureus	C.Albicans	A.Niger
1.	SB1	14 mm	13 mm	16 mm	15 mm
2.	SB1- Cu complex	19 mm	18 mm	19 mm	17 mm
3.	Control	08 mm	08 mm	08 mm	08 mm
4.	Standard	20 mm	20 mm	20 mm	20 mm

The pharmacological activity of all the isolated Schiff base ligand and mixed ligand acac compounds were studied by screening were done in vitro cup diffusion methods. The zone of inhibition around the bore was measured after 24 hr. The antimicrobial activities are classified as standards (=20 mm), highly active results were observed for complex both for antibacterial and antifungal activities.

IV. CONCLUSIONS

In the current study, the main emphasis is on the preparation of bioactive ligands of 4-aminophenol moiety and its complexity. The various spectroscopic techniques were used to elucidate the molecular structure and geometry of the metal complexes. The results exhibit that the synthesized ligand binds with metal ions in tetra dentate through N donor sites of aminophenol as well as O atom of the salicylaldehyde group. IR, UV, ^{1}H NMR, TGA and XRD studies of the complexes also helped to characterize the complexes. Based on all the above spectral studies, a six coordinated octahedral geometry for this complex has been proposed. The antibacterial data show that the metal complex has biological activity and cytotoxic properties. The Schiff base ligand and its complex were also tested for their antibacterial activity to assess their inhibiting potential against, Escherichia. Coli (a gram-negative bacteria) and Staphylococcus aureus (as gram-positive bacteria) using two different concentrations (5 and 10 mm). The results showed the Cu(II) complex has a better rate of anti-bacterial activity with gentamicin as a standard drug. Compared to ligand, copper complex is shown to have very good activity both in antibacterial and antifungal on compared to the standard and control. Higher the number of hydrogen bonds betters the specificity of the ligand with the target protein. Mixed ligand complexes of SB1-acac showed a better chelate effect than SB1- metal salt complexes. The smear pattern of DNA binding studies revealed that the SB1 complex can cleave DNA.

V. ACKNOWLEDGMENTS

One of the authors (**Sridevi S P**) is highly thankful to Raman Research Institute and Indian Institute of Science, Bangalore for getting spectroscopic data, also grateful to the Department of Biotechnology of PES University and Azyme Biosciences for the biological activity. CRG thanks Nrupatunga university/Government Science College for the support. The authors are grateful to SAIF IIT Chennai for data collection and Sapala Organics, Hyderabad. The authors are also grateful to **Dr. Murali Krishna** of Ramaiah Institution of Technology for their support to understand biological studies.

IARJSET ISSN (O) 2393-8021, ISSN (P) 2394-

International Advanced Research Journal in Science, Engineering and Technology

Impact Factor 7.105 ⁜ Vol. 9, Issue 2, February 2022

DOI: 10.17148/IARJSET.2022.9263

VI. REFERENCES:

[1] Karimkakari, Ali Ehsani, in interface science and Technology, 2019.
[2]Brian Birmingham, Aso Kumar Buvanendran, in Practical Management of Pan (fifth Edition), 2014.
[3] Andelka B. Kovacevic, Sergio M. C. Sitva and Slavomira Doktorovova [Pg 103-13], Emerging Nanotechnologies in Immunology, 2018.
[4] L. Viganor, O. Howe, P. McCarron, M. McCann, M. Devereus, Md. Chem. 17 (2017) 1280-1302.
[5] M. Wehbe, A. W. Leung, M. J. Abrams, C. Orvig, M.B. Bally, Daltin Trans. 46 (2017) 10758-10773.
[6] M. Chaurasia, D. Tomar, S. Chandra, J. Mol. Struct. 1179 (2019) 431-442
[7] J. J. Zhang, H.J. Zhou, A. Lachgar, Angew. Chem. 46 (26) (2007) 4995-4998.
[8] H.M Ghasem, S. F. I. Mertens, M. Ghorbani, M. R. Archadi, Mater, Chem. Phys. 78 (3) (2003) 800-808.
[9] N. Allard, S. Beaupr´e, B.R. Aïch, A. Najari, Y. Tao, M. Leclerc, Macromolecules 44 (2011) 7184–7187.
[10] G. Kornis, I. Katritzky, A. R., Pergamon, New York, (1984).
[11] L.J. Lombardo, F.Y. Lee, P. Chen, D. Norris, J.C. Barrish, K. Behnia, S. Castaneda, L. A.M. Cornelius, J. Das, A.M. Doweyko, C. Fairchild, J.T. Hunt, I. Inigo, K. Johnston, A. Kamath, D. Kan, H. Klei, P. Marathe, S. Pang, R. Peterson, S. Pitt, G.L. Schieven, R.J. Schmidt, J. Tokarski, M. Wen, J. Wityak, R.M. Borzilleri, J. Med. Chem. 47 (2004) 6658–6661.
[12] R.R. Zaky, T.A. Yousef, J. Mol. Str. 1002 (2011) 76–85.
[13] Y. Lu, C.M. Li, Z. Wang, C.R. Ross, J. Chen, J.T. Dalton, W. Li, D.D. Miller, J. Med. Chem. 52 (2009) 1701–1711.
[14] E. Khan, Z. Gul, A. Shahzad, S.M. Jan, F. Ullah, M.N. Tahir, J. Coord. Chem. 70 (2017) 4054–4069.
[15] C. Santini, M. Pellei, V. Gandin, M. Porchia, F. Tisato, C. Marzano, Chem. Rev. 114 (2014) 815–862.
[16] G.Y. Nagesh, K. Mahendra Raj, B.H.M. Mruthyumjayaswamy, J. Mol. struct. 1079 (2015) 423–432.
[17] M. Grus, B. Therien, G.S. Fink, A. Casini, F. Edate, P.J. Dyson, J. Organomet. Chem. 695 (2010) 1119–1125.
[18] J.C. Milne, R.S. Roy, A.C. Eliot, N.L. Kelleher, A. Wokhlu, B. Nickels, C.T. Wals, Biochemistry 38 (1999) 4768–4781.
[19] K. Sampath, S. Sathiyaraj, C. Jayabalakrishnan, Med. Chem. Res. 23 (2014) 958–968.
[20] "Antifungal and antibacterial effects of phenolic substances with different alkyl groups. A study of the relation between the biological activity and the constitution of the investigated compounds." Acta Universitatis Palackinanae Olomucensis, Facultatis Medical. (1979), 74: 83-101.
[21] Watanabe, Kuzuko, Ohta, Toshihiro, Shirasu &Yasuhika (1989). "Enhancement and inhibition of mutation by O-Vanillin in Escherichia coli". Mutation Research, DNA repair. 218(2):105-9.
[22] S. Magaldi, S. Mata-Essayag, C. Hartung de Capriles, et al. Well diffusion for antifungal susceptibility testing. Int. J. Infect. Dis., 8 (2004), pp. 39-45
[23] Valgas, C., Souza, S. M. de, Smania, E. F. A., & Smania Jr., A. Screening methods to determine antibacterial activity of natural products. Brazilian Journal of Microbiology (2007) 38: 369–380.
[24] Aydin Tavamn, Serkan Ikiz, Funda Bagcigil A, Yakut Ozgur N &Seyyal AK J. Serb. Chem. Soc. 74 (5) 537–548 (2009)
[25] S.K. Wolff, D.J. Grimwood, J.J. McKinnon, M.J. Turner, D. Jayatilaka, M.A. Spackman, Crystal Explorer (Version 3.1), University of Western Australia, (2012).
[26] M.A. Spackman, J.J. McKinnon, D. Jayatilaka, Electrostatic potentials mapped on Hirshfeld surfaces provide direct insightinto intermolecular interactions in crystals, Cryst. Eng. Comm. 10 (4) (2008) 377– 388.
[27] D. Jayatilaka, D.J. Grimwood, A. Lee, A. Lemay, A.J. Russel, C. Taylo, S.K. Wolff, TONTO-A System for Computational Chemistry, The University of Western Australia, Nedlands, Australia, 2005.
[28] N.R.Sreenatha ,B.N.Lakshminarayana ,D.P.Ganesha ,C.R.Gnanendra ,Crystal structure and Hirshfeld surface analysis of (E)-1-(3,5-dichloro-2-hydroxyphenyl)-3-(5-methyl-furan-2-yl) prop-2-en-1-one, Acta Cryst. E74 (2018) 1451–1454.

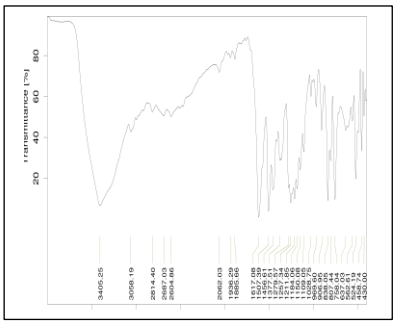

Fig 1: SB1 ligand IR

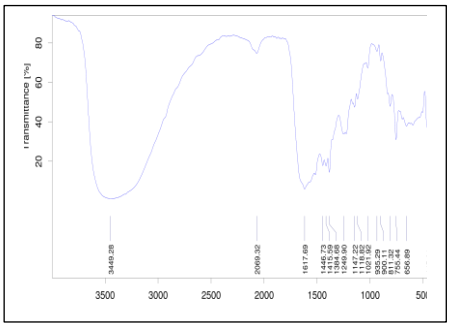

SB1- Ni complex IR

IARJSET ISSN (O) 2393-8021, ISSN (P) 2394-

International Advanced Research Journal in Science, Engineering and Technology

Impact Factor 7.105 ⁜ Vol. 9, Issue 2, February 2022

DOI: 10.17148/IARJSET.2022.9263

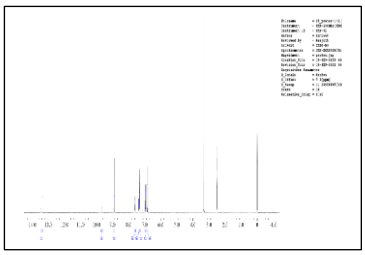

Fig 2: SB 1- NMR

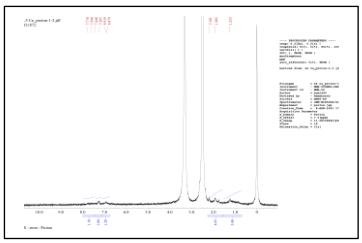

SB1-Ni complex NMR